Air Flow and Particle Trajectories around Aircraft Fuselages. IV: Orientation of Ice Crystals

W. D. KING*

*National Center for Atmospheric Research,** Boulder, CO 80307*

(Manuscript received 6 May 1985, in final form 21 December 1985)

ABSTRACT

The equations of motion for an ice crystal moving around a body are simplified and used to obtain the preferred angular orientation of the crystals with respect to the body. It is shown that the calculated orientation angles are in good agreement with those measured by under-wing probes, and that the major cause of the preferential orientation of columns is the vortex generated at the tips of finite wings. It is also shown that a preferred orientation can be found in data obtained using fuselage-mounted probes, but there the agreement between the calculated and observed angles is not as good.

1. Introduction

At a recent symposium on measurements of cloud particles from aircraft (Baumgardner and Dye, 1982) attention was drawn to observations showing a preferred orientation of ice columns as recorded by the PMS-2D-C[1] imaging probes mounted at wing-tip locations on the King Air research aircraft operated by NCAR and the University of Wyoming. Examples of such images can be found in Gordon and Marwitz (1984) and Baumgardner (1983), and a selection is shown in Fig. 1 (Baumgardner, 1983). Since it would be expected that columns free-falling in cloud would have their major axes randomly oriented in the horizontal plane, the strong preferential orientation at an axis angle of about 60° (see Fig. 2) requires explanation.

In this paper we show first that this particular phenomenon can be explained in terms of a characteristic feature of flow around finite wings. We also note that the occurrence of oriented crystals is not restricted to wing-tip sampling, and indeed could be expected to occur when sampling in any flow-distorted region.

The problem itself should not be viewed in isolation as a sampling idiosyncrasy. It is important to be able to understand the phenomenon itself, since without such an understanding derived quantities such as crystal concentrations, size distributions, etc., could be in error. These errors could arise because the 2-D probes provide information on sizes projected on to a single plane. Any rotation of the crystals around an axis within that plane will produce unfaithful images which would be unnoticeable unless recorded by another probe set up to view an orthogonal plane. For example, the images shown in Fig. 1 could be much shorter than the true lengths of the columns if there had been any rotation about an axis in the plane of the image.

2. Orientation of particles in accelerating air flows

If the laser beam of the imaging probe is aligned vertically (i.e., parallel to the y axis of Fig. 3), then the image as recorded is the shadow of the crystal projected on to the x–z plane. This is the conventional arrangement for most 2-D probes, since it could be expected to provide the maximum information on plate and column shapes if they fall with their major length dimension in the horizontal plane. We will consider orientation effects as detected by probes in other possible configurations later. I have shown in Part III of this series of papers (King, 1985a) that for columns less than 1 mm in length traveling on nonimpacting trajectories around fuselages, the local Reynolds number is always less than 600 and more typically about 100. For this Reynolds number regime it was shown that the aerodynamic torque on the crystal is sufficiently large for it to be in the equilibrium orientation, i.e., with its maximum cross-sectional area across the drag vector which in turn is determined by the direction of the local particle velocity relative to air. For the moment we will assume that the conditions apply here and leave examination of this assumption until later. If **Q** is the air velocity and **U** the particle velocity, then the orientation of the crystal is therefore determined by the local direction of **Q**-**U** along a trajectory. Thus the angle θ of the projection in the x–z plane (see Fig. 1) would be given by

$$\cot\theta = \frac{Q_z - U_z}{Q_x - U_x}. \tag{1}$$

* Permanent affiliation: Cloud Physics Laboratory, Division of Atmospheric Research, CSIRO, Sydney, Australia.

** The National Center for Atmospheric Research is sponsored by the National Science Foundation.

[1] Manufactured by Particle Measuring Systems, Boulder, CO.

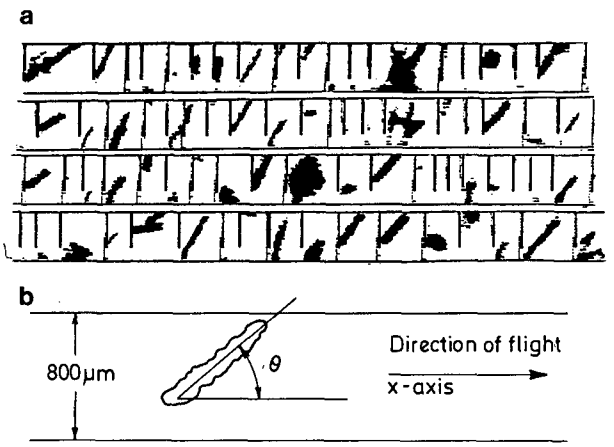

FIG. 1. (a) Images of columns obtained from a starboard wing tip mounting of a 2-D-C probe. (b) Definition of θ (from Baumgardner, 1983).

Note that Fig. 1 does not allow us to unambiguously resolve the direction of the drag vector; we are unable to determine whether the crystal is accelerating or decelerating on a line at right angles to the axis of the crystal.

In this paper we will take our axes as fixed in the aircraft (see Fig. 3), which is considered to be stationary, with the air and particles moving past in the positive x direction. We will also be assuming that steady-state airflow conditions prevail, and that the only variables which depend explicitly on time are the particle velocity and position. For reasons of conceptual convenience our approach commences as Lagrangian (as in the description of the equation of motion) but ends up as essentially Eulerian.

3. Equation of motion

In dimensionless terms the equation of motion of the column can be written as (King, 1985a)

$$\frac{d\mathbf{u}}{d\tau} = \frac{C_d \,\mathrm{Re}}{24\mathrm{S}}(\mathbf{q} - \mathbf{u}) - \mathrm{F}\hat{\mathbf{y}}, \tag{2}$$

where $\mathbf{u}$ is the particle velocity normalized to the free-stream velocity V, τ is the time scale obtained by taking a length scale s divided by V, C_d is the drag coefficient, Re the local Reynolds number, and S and Fr dimensionless Stokes and Froude numbers given by

$$\mathrm{S} = \frac{mdV}{12A\eta s}, \tag{3}$$

where m is the particle mass, d the characteristic length, A the cross-sectional area, and η the air viscosity, and by

$$\mathrm{Fr} = gs/V^2, \tag{4}$$

where g is the gravitational acceleration. Now use of (2) in component form, followed by substitution into (1) yields,

$$\cot\theta = \frac{du_z/d\tau}{du_x/d\tau}, \tag{5}$$

so that the equilibrium orientation angle of a crystal is determined by the ratio of the accelerations it experiences in the two orthogonal directions within the projection plane. This approach, of course, is not new. In fact, 10 years ago Norment (1975) calculated the trajectories of columns moving around the side of a C130E aircraft and then used (5) to calculate the orientation angles.

Unfortunately, this approach is demanding on computer power without providing much information about the important parameters of the orientation mechanism. However for the particular problem at hand, there are some important analytic simplifications which can be made. These simplifications allow us to see quite clearly which are the orientation producing variables, as well as eliminating the need for a full numerical treatment.

Following on from (5), we first note that because u_z is a function of $x(\tau)$, $y(\tau)$ and $z(\tau)$, then

$$\frac{du_z}{d\tau} = \frac{\partial u_z}{\partial x}\frac{dx}{d\tau} + \frac{\partial u_z}{\partial y}\frac{dy}{d\tau} + \frac{\partial u_z}{\partial z}\frac{dz}{d\tau}, \tag{6}$$

$$\approx \frac{\partial u_z}{\partial x}\frac{dx}{d\tau}, \tag{7}$$

since $dx/d\tau > dy/d\tau$, $dz/d\tau$ ahead of slender bodies such as wings, etc. With a similar expression for $du_x/d\tau$, we then have

$$\cot\theta = \frac{\partial u_z/\partial x}{\partial u_x/\partial x}. \tag{8}$$

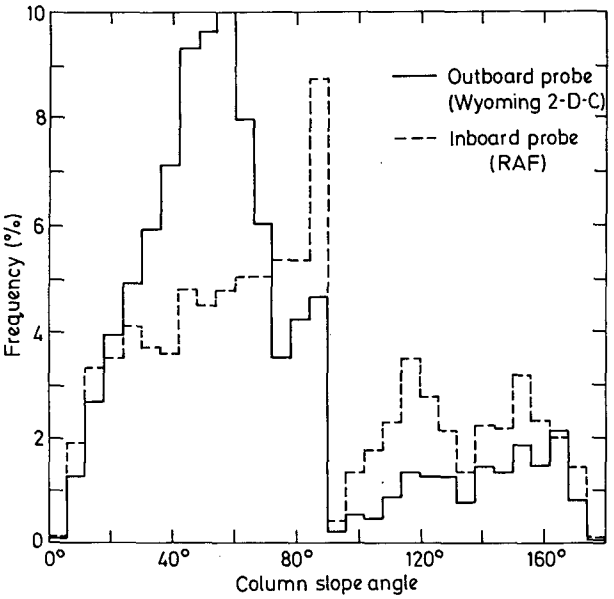

FIG. 2. This histogram shows the frequency at which columnar habits assumed orientation angles between 0° and 180° (from Baumgardner, 1983).

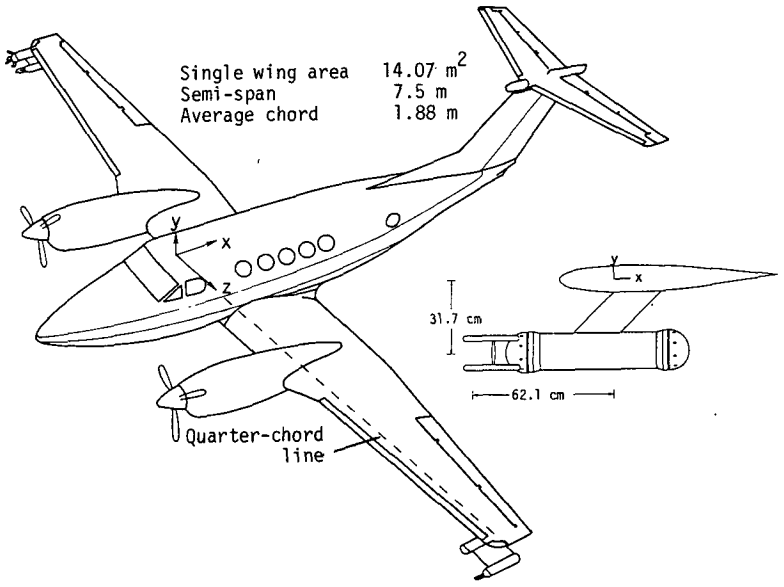

FIG. 3. Coordinate system and detail of sampling location on port wing tip.

Now in many situations related to aircraft sampling of cloud particles the particle velocity **u** is not very different from the air velocity **q** (particularly at small values of S), and we are able to show in appendix A that it is possible to replace the derivatives of **u** in (8) with derivatives of **q**, a step which allows for some substantial simplifications to be made. It is sufficient to note here that for the situation of direct interest to us, i.e., flow ahead of wings, the approximation is a good one to make. Thus we arrive at

$$\cot\theta = \frac{\partial q_z/\partial x}{\partial q_x/\partial x}. \tag{9}$$

It is a consequence of (9) that the orientation angle (a Lagrangian-type parameter) is determined by the ratio of the spatial derivatives of the air velocity in the two orthogonal directions (i.e., Eulerian properties of the velocity field). Note that the direction of the air streamlines is determined by $\tan^{-1}(q_z/q_x)$, etc., and that it is quite possible for this angle to remain small even though θ may be appreciably larger. We return to this later.

It is important to realize that equating the spatial derivatives of **u** and **q** is not inconsistent with the fact that **u** and **q** can differ by a constant amount which provides the drag force and torque on the particle. This concept is explored further in appendix A.

4. Flow around wing tips

It is well known that the lifting action of a finite wing generates line vortices which are shed from the trailing edge of the wing. Together with the bound vortex lines along the span, they constitute a series of horseshoe vortices which are closed at $x = \infty$ by the vortices shed when the wing is initially set in motion. For a wing with elliptic loading the trailing vortex elements have maximum strength at the wing tips, and for many applications the vortex system can be considered to be made up of two trailing wing-tip vortices of circulation Γ joined by a vortex of similar strength along the span at the quarter-chord point. The strength of the line vortex elements is determined by the lift characteristics of the wing via standard aerodynamic theory, but we shall show that the absolute magnitude of Γ is only of secondary importance for the problem at hand. For a horseshoe vortex system the normalized induced velocity components are given by (Milne-Thomson, 1966, p. 178)

$$q_x = \frac{\Gamma y}{4\pi Vc(x^2+y^2)}\left\{\frac{(z+a)}{[x^2+y^2+(z+a)^2]^{1/2}} - \frac{(z-a)}{[x^2+y^2+(z-a)^2]^{1/2}}\right\}, \tag{10}$$

$$q_y = \frac{\Gamma(z-a)}{4\pi Vc[y^2+(z-a)^2]}\left\{1+\frac{x}{[x^2+y^2+(z-a)^2]^{1/2}}\right\} - \frac{\Gamma(z+a)}{4\pi Vc^2[y^2+(z+a)^2]}\left\{1+\frac{x}{[x^2+y^2+(z+a)^2]^{1/2}}\right\}$$
$$- \frac{\Gamma x}{4\pi Vc(x^2+y^2)}\left\{\frac{(z+a)}{[x^2+y^2+(z+a)^2]^{1/2}} - \frac{(z-a)}{[x^2+y^2+(z-a)^2]^{1/2}}\right\}, \tag{11}$$

$$q_z = \frac{\Gamma y}{4\pi Vc[y^2 + (z+a)^2]}\left\{1 + \frac{x}{[x^2 + y^2 + (z+a)^2]^{1/2}}\right\} - \frac{\Gamma y}{4\pi Vc[y^2 + (z-a)^2]}\left\{1 + \frac{x}{[x^2 + y^2 + (z-a)^2]^{1/2}}\right\}. \quad (12)$$

In (10)–(12) the length scale is normalized to the chord length c, and a is the ratio of the wing semi-span to the chord length. Thus in this coordinate system the leading edge at the wing tip is at $x = -0.25$, $y = 0$, $z = a$. The magnitude of velocities calculated using (10) to (12) compare favorably with tip vortex velocity distributions as measured by Chigier and Corsiglia (1971), but the ultimate justification for using such a simple description of the complex flow around wing tips is that it produces surprisingly accurate results for the problem at hand.

With these expressions for the velocity field it is then a simple matter to evaluate the spatial derivatives $\partial q_x/\partial x$, etc., for substitution into (9), allowing the equilibrium orientation angle to be calculated for any position in space. Figure 4 shows this angle calculated as a function of distance ahead of the wing for particles which pass a distance $y = -0.17$ below the wing under the tip. This is the position of the outboard 2-D probe on the King Air, and corresponds to that position at which the data of Figs. 1 and 2 were obtained. There are several features worth noting from this figure and from the form of Eqs. (9)–(12):

(i) The calculated orientation angle at the wing tip is close to that measured from the images of Fig. 1 (see Fig. 2).

(ii) The calculated angle is sensitive to distance ahead of the wing, and distance inboard. Figure 4 shows that the region where the orientation angle is 60° is confined very much to the wing-tip location. Movement of the probe to $y = -0.133$, $z = 3.67$ (corresponding to the inboard probe position on the King Air) produces an increase in the calculated angle from 60° to 83°. This also agrees well with the experimental data as shown in Fig. 2.

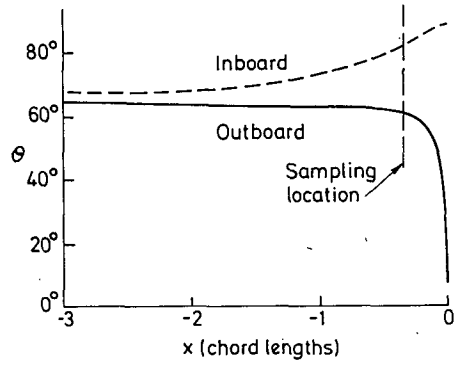

FIG. 4. Equilibrium orientation angle as a function of distance ahead of the quarter-chord line.

(iii) The orientation angle in the x–z plane is independent of aircraft speed, lift characteristics, etc., because Γ cancels in taking the ratio of the derivatives. Thus, although there may be more or less vorticity than calculated from aerodynamic theory because of the effects of real wings, blockages, etc., as long as the spatial variation is similar to that described by (10)–(12) the results are independent of the absolute value of Γ. It is for this reason that such a simple model as the horseshoe vortex can yield such surprisingly accurate predictions. To a lesser extent the magnitude of the effect will also be insensitive to aircraft type because of the weak dependence on a, the ratio of span to chord length.

(iv) The angle is independent of crystal size. This is an inherent result of the model because of the assumption that $\mathbf{q} \approx \mathbf{v}$ for all particles, but the analytical and numerical treatments of appendix A support this at sampling locations ahead of the wing.

(v) The orientation angles are much greater than the angle that the air streamlines make with the x axis, calculated as $\tan^{-1}(q_z/q_x)$. For the King Air with an all-up mass of 5800 kg moving at a velocity of 80 m s^{-1} this angle is of the order of 1° at the outboard sampling location. The fact that this angle is small is in line with tufting observations by Baumgardner (personal communication, 1984). Note that these streamline angles are aircraft- and lift-dependent but are always quite small ahead of the wing.

5. Other probe configurations and positions

a. Horizontal orientation of laser beam

For a 2-D probe installed such that the laser beam was in the horizontal plane (this would be desirable, for example, when examining the "side-on" shapes of conical graupel, etc.), the image is the shadow projected on to the x–y plane. With this system, plates would presumably appear as rectangles, with the axis of the rectangle horizontal in the absence of flow distortion effects and tilted if in a region of accelerating air flow. In this last case the angle of tilt α would be given by $\cot^{-1}(q_y - u_y)/(q_x - u_x)$. Using the same arguments as before, we can simplify to

$$\alpha = \cot^{-1}\left[\frac{\partial q_y/\partial x}{\partial q_x/\partial x} + \frac{\mathrm{Fr}}{\partial q_x/\partial x}\right], \quad (13)$$

where the term involving Fr arises because of the effects of gravity. In this case it is flow over or under the wings

which causes the tilt, and although the angle of tilt will depend on the lift coefficient of the wing because Γ no longer cancels completely, this turns out to be a minor effect at the sampling position where $\partial q_y/\partial x \gg \mathrm{Fr}$.

Values of α computed from (13) are shown in Fig. 5 for the wing-tip position and for the mid-span position. Unlike θ, α shows little variation in the spanwise direction, the reason being that α is dominated by the bound vortex of constant strength in the horseshoe vortex model. The fact that α is quite large at the sampling location suggests that (i) again it should be comparatively easy to compare with experimental data should any become available and (ii) allowances should be made for this angle in computing the sizes of plates and columns from their projection in the x–z plane.

b. *Fuselage mounts*

An examination of (9) quickly shows that the phenomenon of a particular orientation of crystals need not be restricted to under-wing mounts—it could occur anywhere where there is acceleration of the airflow. While the equilibrium angle is given by (9), whether it attains this angle depends on whether the flow distortions in the two orthogonal directions are in phase (see appendix A) and whether the particle spends sufficient time in the flow-distorted region (see appendix B). With regard to fuselage mounts, the first condition is generally not satisfied because behind the cockpit q_x and q_z are in antiphase, i.e., q_x is decreasing while q_z is increasing (see Fig. 1 of King, 1984). Under these conditions it is not sufficient to use the simple treatment implied in (9). Rather, a full numerical solution must be obtained so that $du_x/d\tau$, etc., can be computed and then θ calculated via (5), as in the approach taken by Norment (1975).

With regard to fuselage mounts we also note that we would expect columns sampled along the line of symmetry of the fuselage (i.e., center top or center bottom) to be aligned with $\theta = \pi/2$ because $du_z/d\tau$ must be zero along this line. As one moves around the side of the fuselage, the angle should decrease. The distribution of orientation angles as measured at a side fuselage mount of an F-27 is given in Fig. 6. The equilibrium angle obtained by evaluating (5) at the sampling location as calculated by numerical integration of the equations of motion (2) is close to 0°. An examination of Fig. 6 shows that there is indeed a peak in the distribution at 0°, but there is also a more substantial one at about −45°, and a minor one at 45°.

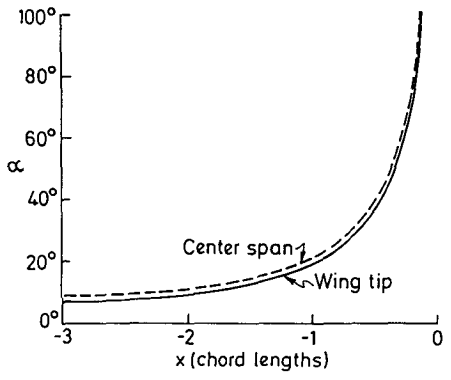

FIG. 5. Equilibrium orientation angle in the x–y plane as a function of distance ahead of the wing.

Thus for the fuselage mounts we do not get very good agreement between the observed and calculated angles. Inspection of the inset to Fig. 6 shows that the sampling position is directly ahead of the F-27 wing (about 1.5 chord lengths) and also not far outside the propeller disk. It seems highly likely that either or both of these flow-disturbing elements could be affecting the orientation angles. In any case, it does not seem feasible to tackle what is obviously a more complex situation than under the wings. In passing, we note that the angles calculated by Norment (1975) using the same technique would also suffer from the same problem if the probe locations were near propellers or wings.

6. Conclusions

It is apparent from the foregoing that aircraft-induced flow distortions can have considerable effects on the reorientation of ice crystals. Although first observed on wing-mounted probes, the effects can be found at any sample location where there are accelerations in the air flow. For most ranges of aircraft sizes, sampling speeds, etc., and for the range of interest of ice crystal sizes, there is sufficient aerodynamic torque to ensure the particles are aligned along the direction of instantaneous drag. In general, this allows for some simplification to be made in calculating the orientation angles. More particular conclusions that can be drawn include

(i) In the x–z plane, the orientation angle is determined by the ratio of the air accelerations in the orthogonal x, z directions.

(ii) For probes under aircraft wings, the effects are maximized near the wing tips, and are largely independent of aircraft size, lift characteristics, etc. Calculated orientation angles agree well with measured ones.

(iii) For probes mounted on fuselages, calculated orientation angles show only moderate agreement with the experimentally measured ones.

Acknowledgments. The author wishes to acknowledge the experimental work of Darrel Baumgardner of NCAR, and John Marwitz and Al Cooper of the University of Wyoming. Their documentation of the problem provided the stimulus for this work, which was performed while the author was on leave from CSIRO at NCAR. It is a pleasure to acknowledge the assistance of Darrel Baumgardner, Jack Warner, and Byron Phil-

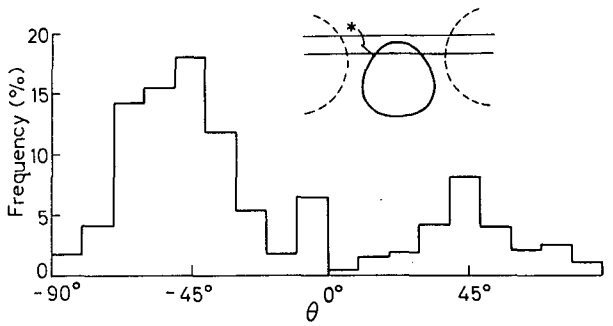

FIG. 6. Measured orientation angles (θ) at the fuselage location shown in the inset by the asterisk.

lips in facilitating that visit. The author also wishes to acknowledge the assistance of Al Drummond of the National Aeronautical Establishment of Canada in clarifying certain aspects of the manuscript. Data from the F-27 were gathered with the help of Michael Macinante and analysed with the assistance of Shui Choo Tan.

APPENDIX A

Estimates of $q_x - u_x$ etc.

In section 3, we made the approximation $\partial u_x/\partial x = \partial q_x/\partial x$ etc. In this appendix we examine the conditions under which such an approximation is useful.

Let us initially confine ourselves to motion in a single direction (x), so that our equation of motion is

$$du_x/d\tau = (q_x - u_x)/\tau_p, \tag{A1}$$

where $\tau_p = (C_d\,\mathrm{Re}/24S)^{-1}$ and can be considered as a basic time constant for the particle's velocity. We shall assume that the particle moves along with a velocity close to the air velocity, but differing from it by an amount $\epsilon_x[x(\tau)]$. Thus we let

$$u_x(\tau) = q_x[x(\tau)] + \epsilon_x[x(\tau)], \tag{A2}$$

where we expect ϵ_x to be small, and then (A1) becomes

$$d\epsilon_x/d\tau + \epsilon_x/\tau_p = -dq_x/d\tau. \tag{A3}$$

Note that $dq_x/d\tau$ is the rate of change of air velocity as felt by the particle as it moves along its trajectory, and is non-zero even though the air flow is considered steady (i.e., $\partial q_x/\partial t = 0$). Thus

$$\frac{dq_x}{d\tau} = \frac{\partial q_x}{\partial x}\frac{dx}{d\tau} \approx \frac{\partial q_x}{\partial x} \tag{A4}$$

because $dx/d\tau \approx 1$. We shall further suppose that in the region of interest, $\partial q_x/\partial x$ is a constant which we shall denote by α_x, where α_x would typically be small and negative for our situations ahead of wings, etc. If we then integrate (A3) forward in time from when the particle is initially at rest with respect to the fluid (i.e., $\epsilon_x = 0$), then the solution is

$$\epsilon_x(\tau) = -(1 - e^{-\tau/\tau_p})\alpha_x\tau_p. \tag{A5}$$

Thus the difference between the air velocity and particle velocity increases with time, approaching a constant value of $-\alpha_x\tau_p$ with a time constant of τ_p. For $\tau \ll \tau_p$, which is generally the case for situations of interest to us, $\epsilon \approx -\alpha_x\tau = \Delta q$, Δq being the change in air velocity from the free-stream value.

If we consider a similar but independent flow in the z direction, but with gradient α_z, then

$$\epsilon_z(\tau) = -(1 - e^{-\tau/\tau_p})\alpha_z\tau_p, \tag{A6}$$

$$\frac{du_z}{d\tau}\Big/\frac{du_x}{d\tau} = \epsilon_z(\tau)/\epsilon_x(\tau) = \alpha_z/\alpha_x, \tag{A7}$$

$$= \frac{\partial q_z}{\partial x}\Big/\frac{\partial q_x}{\partial x}, \tag{A8}$$

thus justifying in simple terms the assumptions of section 3. As further proof we present in Fig. A1 a comparison between orientation angles based on the simple expression of (9) and those calculated from full numerical integration of the equations of motion in the manner described by King (1985a). It can be seen that the differences between the two are quite small. This can be shown to be true even for columns as large as 1 mm diameter and 2 mm long.

For the more general case for flow around an obstacle where there could be local maxima in air velocity (such as around fuselages, etc.), it would be more appropriate to take

$$q_x[x(\tau)] = 1 + \alpha_x x + \beta_x x^2, \tag{A9}$$

where α_x, β_x would be of opposite sign. Then the solution to (A3) is

$$\epsilon_x(\tau) = -(1 - e^{-\tau/\tau_p})(\alpha_x\tau_p - 2\beta_x\tau_p^2) + 2\beta_x\tau_p\tau. \tag{A10}$$

With a similar solution for $\epsilon_z(\tau)$ we note that

$$\frac{\epsilon_z}{\epsilon_x} \neq \frac{\alpha_z + 2\beta_z\tau}{\alpha_x + 2\beta_x\tau}, \tag{A11}$$

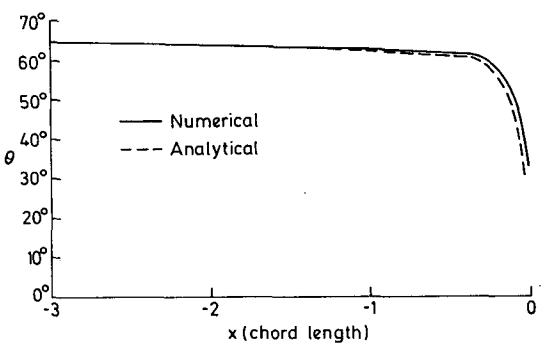

FIG. A1. A comparison between the full numerical solution for θ and the solution obtained analytically. The numerical solution was calculated for a crystal with $l = 700\ \mu$m, $d = 350\ \mu$m, $\rho_p = 5 \times 10^2$ kg m^{-3}, and the aircraft flying with a mass of 5800 kg at 700 mb and a true airspeed of 80 m s^{-1}.

which would be required to make the simplifying substitution set forth in section 3. Thus we could not expect (9) to predict the correct orientation angles if the flow is of a form described by (A9). In general terms, a description of the type of (A9) is required when looking at flows close to or behind the disturbance region, whereas the simpler form is generally adequate when looking ahead of the disturbance. It is for this reason that (9) gives such a good description of the orientation angles ahead of wings, but is not adequate for areas behind the cockpit region of the fuselage.

APPENDIX B

Rotational Time Constants

In this appendix we show that columns have sufficient time to move from a random orientation in the x–z plane to the equilibrium angles calculated using (8).

King (1985a) has shown that the fundamental rotation rate θ for a column is of the order of

$$\dot{\theta} \approx \left(\frac{\rho_a}{\rho_c}\right)^{1/2} \frac{\mathrm{Re}\eta}{ld\rho_a}, \tag{B1}$$

where ρ_a, ρ_c are the densities of air and column respectively, and l, d are respectively the length and diameter of the column. This relationship was derived using the moment of inertia of a column and a fraction ($\frac{1}{10}$) of the torque calculated from potential flow theory. It is considered accurate to within a factor of three, but is only applicable when $\mathrm{Re} \gg 1$, since columns have sufficient symmetry to translate at any orientation with respect to the flow if $\mathrm{Re} \ll 1$ (Happel and Brenner, 1965). We shall assume (B1) is appropriate for $\mathrm{Re} \geq 3$.

Now Re can be estimated as a function of the distance ahead of the wing from the calculation of ϵ_x given in appendix A, since $\mathrm{Re} = \epsilon U\rho_a d/\eta$. For $\tau < \tau_p$ it is shown there that

$$\epsilon_x = q_x(-\infty) - q_x(x) \tag{B2}$$

$$= \frac{\Gamma y}{4\pi V c x^2} \tag{B3}$$

from (9). Standard aerodynamic theory for finite wings gives

$$\Gamma = 2m_a g/(\rho_a U \pi s), \tag{B4}$$

where m_a is the mass of the aircraft and s the wing semispan. Taking $m_a = 5580$ kg, $s = 7.5$ m, $\rho_a = 0.9$ kg m^{-3}, and $U = 80$ m s^{-1}, we have $\Gamma = 65$ m^2 s^{-1}. Thus for a crystal 100 μm in diameter, the Reynolds number exceeds 3 when $x > -0.9$, for a 200-μm crystal when $x > -1.26$, etc. We therefore see immediately that for most crystals that part of the curve of Fig. 4 ahead of $x \approx -1$ has little meaning; crystals of typical size will have insufficient torque in this region to move them towards the equilibrium position. It is only when they are within a chord length of the wing that they will be able to rotate to the equilibrium position.

The total angle through which a crystal can move is found by integrating (B1) to be

$$\Delta\theta = \left(\frac{\rho_a}{\rho_c}\right)^{1/2} \left(\frac{c}{l}\right) \Gamma y \left(\frac{1}{x_i} - \frac{1}{x}\right), \tag{B5}$$

where c is the wing chord, x_i the position at which the Reynolds number exceeds 3 as above, and x the final position. Taking $\rho_c = 5 \times 10^2$ kg m^{-3}, $c = 1.88$ m, $l = 500$ μm, $x = -0.33$, $y = 0.17$, and $x_i = -1.0$ from above, then $\Delta\theta \approx 100°$. Since at most a crystal should have to rotate through 90° to assume the equilibrium position, we see that it should indeed be able to do so.

An exactly analogous analysis can be performed with respect to the flow around the canister housing the 2-D probe. For this canister,

$$\epsilon = r_c^2/4(X^2 + r_c)^2 \tag{B6}$$

(King, 1985b), where r_c is the radius of the hemispherical cap and X the distance ahead of the nose of the canister measured from a position $r_c/2$ behind the nose. For this geometry, $\mathrm{Re} \approx 3$ when $X/r_c \approx 5.6$, i.e., about 40 cm ahead of the pod. Since the sampling point is 15 cm ahead of the pod a crystal has only 25 cm in which to realign compared with 130 cm for the wing lift disturbance. It is for this reason that the equilibrium angle calculated due to the wing lift alone is the appropriate angle, even though the decelerations due to the wing and pod at the sampling position are of similar magnitude. This conclusion is similar to the one arrived at by Beard (1983) in considering the effect of the canister on the canting angles of graupel particles.

The same arguments can also be used to show that the flow distortion caused by the shape of the wing (as opposed by its lift characteristics described by (10)–(12) can also be ignored in terms of reorientation of columns.

REFERENCES

Baumgardner, D., 1983: Airflow induced rotation of ice particles. NCAR *Newslett., Dev. Airborne Cloud Phys. Instrum.* J. Dye, Ed., June, 4–6.

——, and J. E. Dye, 1982: *Cloud Particle Measurement Symposium: Summaries and Abstracts.* NCAR Tech. Note TN-199, 103 pp.

Beard, K. V., 1983: Reorientation of hydrometeors in aircraft accelerated flow. *J. Climate Appl. Meteor.*, **22**, 1961–1963.

Chigier, N. A., and V. R. Corsiglia, 1971: Tip vortices–velocity distributions. 27th Annual National VSTOL Forum, Amer. Helicopter Soc. Preprint No. 522, 13 pp.

Gordon, G. L., and J. D. Marwitz, 1984: An airborne comparison of three PMS probes. *J. Atmos. Oceanic Technol.*, **1**, 22–27.

Happel, J., and H. Brenner, 1965: *Low Reynolds Number Hydrodynamics.* Prentice-Hall, 553 pp.

King, W. D., 1984: Air flow and particle trajectories around aircraft fuselages. I: Theory. *J. Atmos. Oceanic Technol.*, **1**, 5–13.

——, 1985a: Air flow and particle trajectories around aircraft fuselages. III: Extensions to particles of arbitrary shape. *J. Atmos. Oceanic Technol.* **2**, 539–547.

——, 1985b: Air flow around PMS canisters. *J. Atmos. Oceanic Technol.*, **3**, 197–198.

Milne-Thomson, L. M., 1966: *Theoretical Aerodynamics.* Macmillan, 430 pp.

Norment, H. G., 1975: Effects of airplane flowfields on cloud water content measurements. Rep. No. AFCRL-TR-75-0231. Air Force Cambridge Research Lab., Hanscom AFB, 72 pp.